

Article

State of Charge Estimation of Lithium-Ion Battery for Electric Vehicles under Extreme Operating Temperatures Based on an Adaptive Temporal Convolutional Network

Jiazhi Miao ^{1,2}, Zheming Tong ^{1,2,*}, Shuiguang Tong ^{1,2}, Jun Zhang ² and Jiale Mao ³

¹ State Key Laboratory of Fluid Power and Mechatronic Systems, Zhejiang University, Hangzhou 310027, China

² School of Mechanical Engineering, Zhejiang University, Hangzhou 310027, China

³ College of Chemical and Biological Engineering, Zhejiang University, Hangzhou 310027, China

* Correspondence: tzm@zju.edu.cn

Abstract: The accurate estimation of state of charge (SOC) under various conditions is critical to the research and application of batteries, especially at extreme temperatures. However, few studies have examined the SOC estimation performance of estimation algorithms for several types of batteries under such conditions. In this study, a new method was derived for SOC estimation and a series of experiments were conducted covering five types of lithium-ion batteries with three kinds of cathode materials (i.e., LiFePO₄, Li(Ni_{0.5}Co_{0.2}Mn_{0.3})O₂, and LiCoO₂), three test temperatures, and four real driving cycles to verify the proposed method. The test temperatures for battery operation ranges from –20 to 60 °C. Then, an adaptive machine learning (ML) framework based on the deep temporal convolutional network (TCN) and Coulomb counting method was proposed, and the structure of the estimation model was designed through the Taguchi method. The accuracy and generalizability of the proposed method were evaluated by calculating the estimation errors and their standard deviations (SDs), its average errors showed a decline of at least 49.66%, and its SDs showed a decline of at least 45.88% when compared to four popular ML methods. These traditional ML methods performed poor accuracy and stability at extreme temperatures (–20 and 60 °C) when compared to 25 °C, while the proposed adaptive method exhibited stable and high performances at different temperatures.

Keywords: machine learning; state of charge estimation; temporal convolutional network; extreme temperature



Citation: Miao, J.; Tong, Z.; Tong, S.; Zhang, J.; Mao, J. State of Charge Estimation of Lithium-Ion Battery for Electric Vehicles under Extreme Operating Temperatures Based on an Adaptive Temporal Convolutional Network. *Batteries* **2022**, *8*, 145. <https://doi.org/10.3390/batteries8100145>

Academic Editor: Matthieu Dubarry

Received: 23 August 2022

Accepted: 23 September 2022

Published: 27 September 2022

Publisher's Note: MDPI stays neutral with regard to jurisdictional claims in published maps and institutional affiliations.



Copyright: © 2022 by the authors. Licensee MDPI, Basel, Switzerland. This article is an open access article distributed under the terms and conditions of the Creative Commons Attribution (CC BY) license (<https://creativecommons.org/licenses/by/4.0/>).

1. Introduction

Recently, environmental pollution has become increasingly serious, with greenhouse gas emissions rising rapidly due to large-scale fossil fuel consumption [1,2]. Therefore, it is important to develop green and clean energy sources, which are efficient and convenient [3,4]. Lithium-ion batteries (LIBs) exhibit high mobility, a long lifespan and high energy-density, which are widely used in clean transportation systems, smart grids, and renewable energy sources [1,5,6]. There are two key methods to accelerate the application of LIBs: (1) Develop new materials with better electrochemical properties, which makes batteries safer, more efficient, and have longer lifespans [7,8]; (2) Higher-accuracy quantification of the internal electrochemical changes of the LIBs from the macroscopic point of view, such that the appropriate operations (e.g., charge, discharge, or maintain) can be decided at any time to ensure that the battery works in a safe and healthy condition [9]. This prompts the real-time estimation of battery health state. The state of charge (SOC) of LIB, as one of the most important indicators of internal battery health state, can show the remaining battery energy and help to formulate an appropriate charge and discharge strategy [10–13].

Since the battery health states including SOC cannot be measured directly through sensors, there has been a tremendous amount of research to develop estimation algo-

rithms for higher accuracy [14–17]. The SOC estimation methods can be divided into three categories: conventional methods, model-based methods, and machine learning (ML) methods [18–21]. The conventional methods include the open circuit voltage (OCV) method [22], the Coulomb counting method [23], and the electrochemical impedance spectroscopy (EIS) method [24,25]. The OCV method estimates the SOC through a one-to-one relationship between the OCV and the SOC [26]; however, it cannot be used for the LiFePO₄ battery because of a flat plateau in the OCV–SOC curve [27]. In addition, a long rest time is needed to make the battery reach an equilibrium condition before measuring the OCV, which limits its online application [28]. The key characteristics of the Coulomb counting method are low computational costs and poor accuracy [18]. The EIS method utilizes the battery impedance and internal resistance to describe the electrical characteristic, but it is expensive [29].

For the model-based approaches, the Kalman filter (KF) and the particle filter (PF) are the most widely used methods [30,31]. Since the KF is more likely to be used for a linear system, while the LIB is a highly nonlinear system, some extensions were proposed to address the adaptivity problem [32]. Xiong et al. [33] used an extended Kalman filter (EKF) to estimate the SOC of the vanadium redox flow battery, and the results showed that the maximum estimation error was within 5.5%. Wang et al. [34] proposed a robust adaptive unscented Kalman filter (UKF) method for unbiased SOC estimation. Their method was applied on a LiNi_xCoyMn_zO₂ battery with a rated capacity of 40 Ah under 25 °C, and the maximum absolute error exceeded 5%. Yang et al. [35] applied a novel fuzzy adaptive cubature Kalman filter (CKF) to estimate the SOC of LIB under 35 °C. The results revealed that this method has a faster convergence speed compared with the traditional CKF method. Wang et al. [36] utilized the PF method to estimate the SOC of the LiFePO₄ battery under a dynamic temperature condition of –3.5 to 45 °C, which showed better performance with less than 1% error compared to EKF.

In contrast, ML methods have become highly attractive in many fields in recent years. For example, they have been used for the prediction of material properties and characteristics [37,38], estimation of battery health states [39,40], and energy storage applications [41]. For SOC estimation, the ML methods treat the battery system as a black box and build the model by fitting the collected data. The commonly used ML methods include support vector machine for regression (SVR) [42], long-short term memory (LSTM) network [43], and convolutional neural network (CNN) [44], as well as the combination of CNN and LSTM. Lu et al. [45] developed a novel deep operator network that has better performance compared to traditional algorithms. In recent years, the temporal convolutional network (TCN) has proved to have excellent performance for the estimation of time series data due to its characteristics of causal convolution, dilation convolution, and residual block [46]. Liu et al. [47] utilized the TCN to estimate the SOC of the LiFePO₄ battery and applied it to the LiPO battery through transfer learning. However, the maximum estimation errors were large at 4.14% under the constant temperature and 10% under rising ambient temperature. In addition, the adaptive activations have proved that they are very helpful to train the neural networks [48]. Jagtap et al. [48–50] have proposed many kinds of adaptive activation functions for regression problems. They provide excellent learning capacity compared to the traditional method.

Despite the above advancements, there are two aspects in the research of SOC estimation that need to be further improved: (1) The generalizability of the algorithm to different types of batteries. This means that improved methods can have a broader range of applications. Many studies only utilize one type of battery to validate their algorithms [26,27,29,30,51], which is not sufficient to prove their generalizability; (2) The adaptability of the algorithm to extreme temperatures. It will be helpful to accelerate the applications of LIB in special situations or extreme environments with high safety and reliability, such as ultra-low temperature cold storage, cold area, and high-temperature workshop. In fact, few studies have validated the estimation performance of the algorithm with the battery working at extreme temperatures, as the testing temperatures in most studies are distributed from –10 to 50 °C [26,27,29,30].

In order to further improve the accuracy and generalizability of estimation algorithms to different types of batteries and extreme temperatures, in this paper, the temporal convolutional network (TCN) is utilized to estimate the SOC of LIBs. Its hyperparameters are optimized by the Taguchi method, and the Coulomb counting method is used to produce the input parameter that is highly related to the SOC for the TCN. To sufficiently prove the generalizability of the proposed method, five types of commonly used batteries are employed, which have three kinds of cathode materials (i.e., LiFePO₄, Li(Ni_{0.5}Co_{0.2}Mn_{0.3})O₂, and LiCoO₂), and they are tested under a constant ambient temperature of 25 °C and two extreme temperatures (−20 and 60 °C), as well as four real driving cycles, including the dynamic stress test (DST), the federal urban driving schedule (FUDS), the urban dynamometer driving schedule (UDDS), and a supplemental federal test procedure driving schedule called US06.

2. Experimental and Methodology

2.1. Experimental Procedure and Dataset

Five types of batteries made from three kinds of cathode materials were utilized to better prove the generalizability of the proposed method in this paper. The detailed battery information is shown in Table 1. The recommended operating temperatures for the five types of batteries were distributed from −20 to 60 °C. To verify the performance of the proposed method under extreme temperatures and its generalizability to different working temperatures, all batteries were tested separately at −20, 25 and 60 °C. To evaluate the performance of the proposed method in practical applications and its generalizability to different conditions, tests with four real driving cycles (i.e., DST, FUDS, UDDS, and US06) were developed. Before performing these tests, peak power tests and OCV tests were performed under different temperatures, with the test strategy shown in Figure 1. The parameters used in peak power test are defined as follows [52]:

$$P_r = I_1 \times V_2 \quad (1)$$

$$I_2 = 80\% \times \frac{P_r}{V_1}, \quad (2)$$

$$V_{limit} = \max(V_1, V_2), \quad (3)$$

$$I_{high} = \min(I_1, I_2), \quad (4)$$

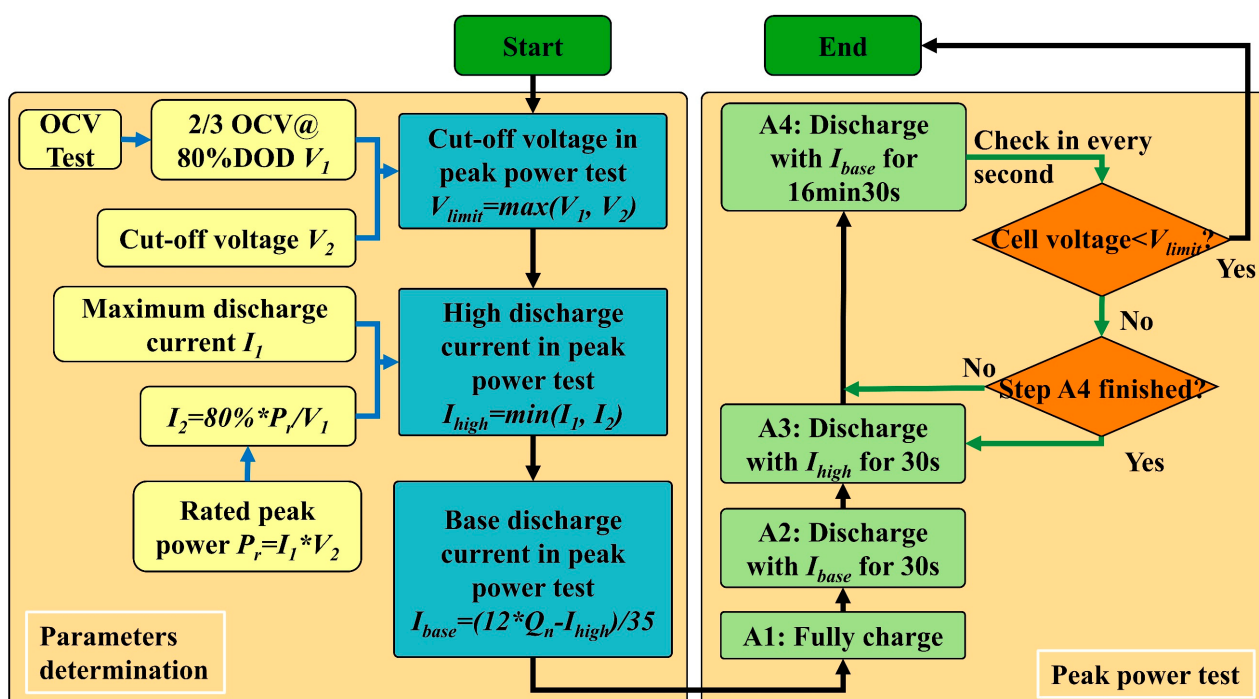
$$I_{base} = \frac{(12 \times Q_n - I_{high})}{35}, \quad (5)$$

where P_r is the rated peak power, I_1 represents the recommended maximum discharge current, V_2 represents the cut-off voltage, I_2 represents the calculated maximum discharge current, V_1 is the 2/3 open circuit voltage at 80% depth of discharge, V_{limit} is the cut-off voltage of the peak power test, I_{high} is the maximum current in the peak power test, Q_n is the rated capacity, and I_{base} is the minimum current in the peak power test.

The detailed information of peak power tests for five types of batteries under different temperatures is shown in Tables S1–S3, and the results are depicted in Figure 2. The peak power declined from 20% to 80% when the battery worked under extreme temperatures (−20 or 60 °C) compared with 25 °C. The current, voltage and temperature were collected every second through the sensors. In summary, the total number of tests reached 90 groups, including 15 groups of OCV tests, 15 groups of peak power tests, and 60 groups of real driving cycle tests. The partial test data were depicted in Figure 3. Importantly, while the temperature increased, the voltage became more stable.

Table 1. Details of five types of battery information.

| Battery Types | Electrode Material | Nominal Capacity (Ah) | Cut-off Voltage (V) | Charging Voltage (V) | Recommended Operating Temperatures |
|---------------|--|-----------------------|---------------------|----------------------|--|
| LR1865EH | LiFePO ₄ /graphite | 1.7 | 2.0 | 3.6 | 0~45 °C (charge); -20~60 °C (discharge) |
| LR1865SK | LiFePO ₄ /graphite | 2.6 | 2.75 | 4.2 | |
| LR1865SZ | LiFePO ₄ /graphite | 2.5 | 3.0 | 4.2 | |
| LR2170SA | Li(Ni _{0.5} Co _{0.2} Mn _{0.3})O ₂ /graphite | 4.0 | 2.75 | 4.2 | |
| ICR18650 | LiCoO ₂ /graphite | 2.55 | 2.5 | 4.2 | |

**Figure 1.** Schematic diagram of the peak power test.

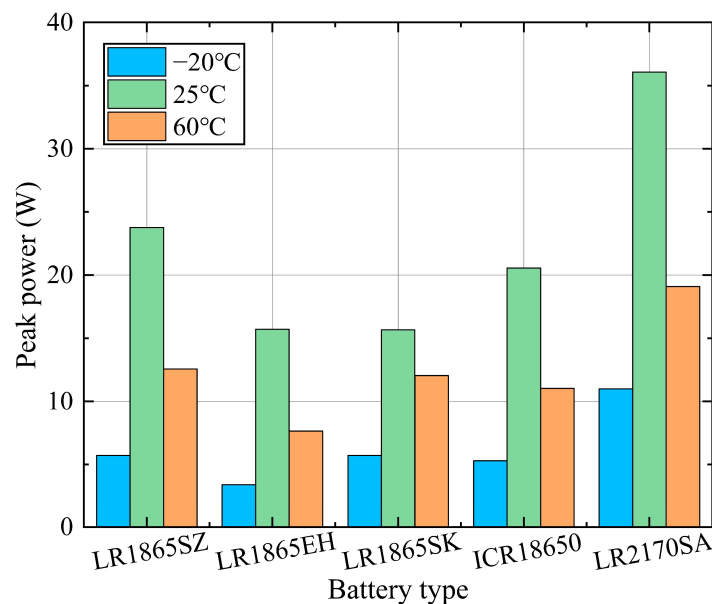


Figure 2. Peak power of different types of batteries (LR1865SZ, LR1865EH, LR1865SK, ICR18650, and LR2170SA) under various temperatures (-20 , 25 and 60 $^{\circ}\text{C}$).

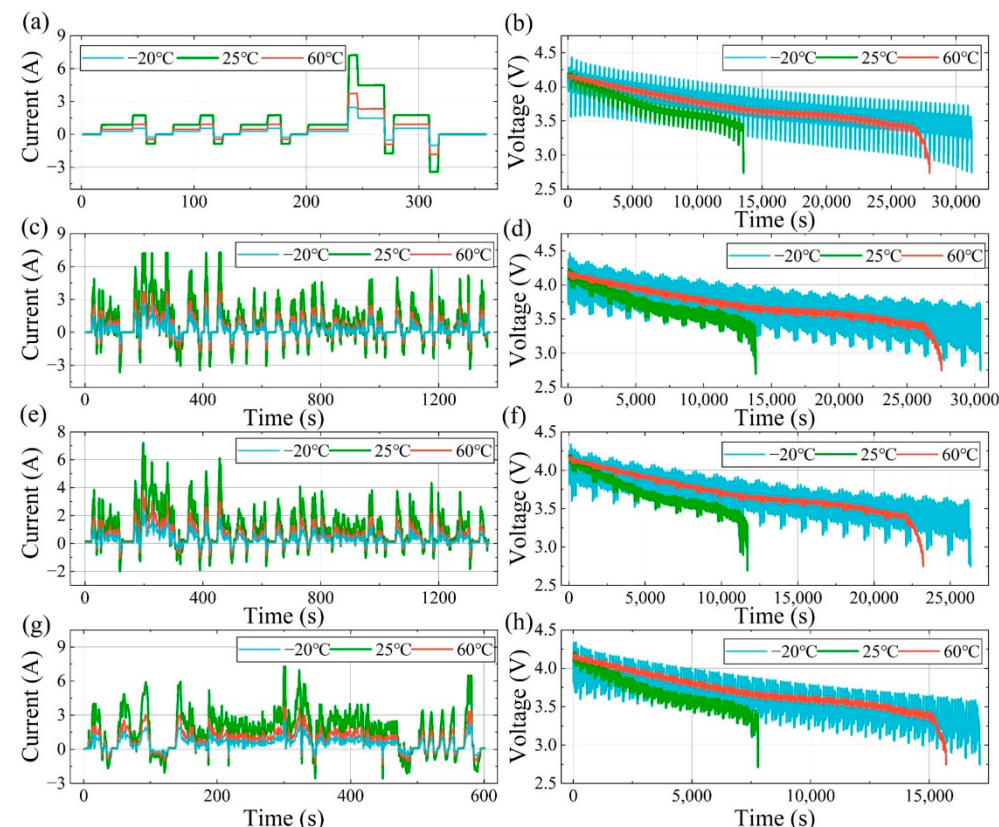


Figure 3. Voltage and current measurement under (a,b) DST, (c,d) FUDS, (e,f) UDDS, and (g,h) US06 experiments for the battery LR2170SA at different temperatures: -20 , 25 , and 60 $^{\circ}\text{C}$.

2.2. Machine Learning

In this paper, the TCN was utilized to estimate the SOC of batteries. The architectural elements in a TCN were shown in Figure 4. Causal convolution makes the method suitable for sequence modeling, which the traditional CNN cannot deal with. Dilated convolution confers the TCN a larger receptive field size with fewer network layers compared to the

traditional CNN; thus, more input data can be considered for every step of SOC estimation. In addition, the utilization of residual blocks can address the vanishing gradient problem of the deep neural network. MAE and RMSE were used to evaluate the performance of the estimation algorithm, which are calculated as:

$$MAE = \frac{1}{n} \sum_{i=1}^n |y_i - \hat{y}_i| \quad (6)$$

$$RMSE = \sqrt{\frac{1}{n} \sum_{i=1}^n (y_i - \hat{y}_i)^2}, \quad (7)$$

where n denotes the total time steps of the real driving cycles, and \hat{y}_i and y_i are the estimated SOC value and the experimental SOC value, respectively, for the i -th time step.

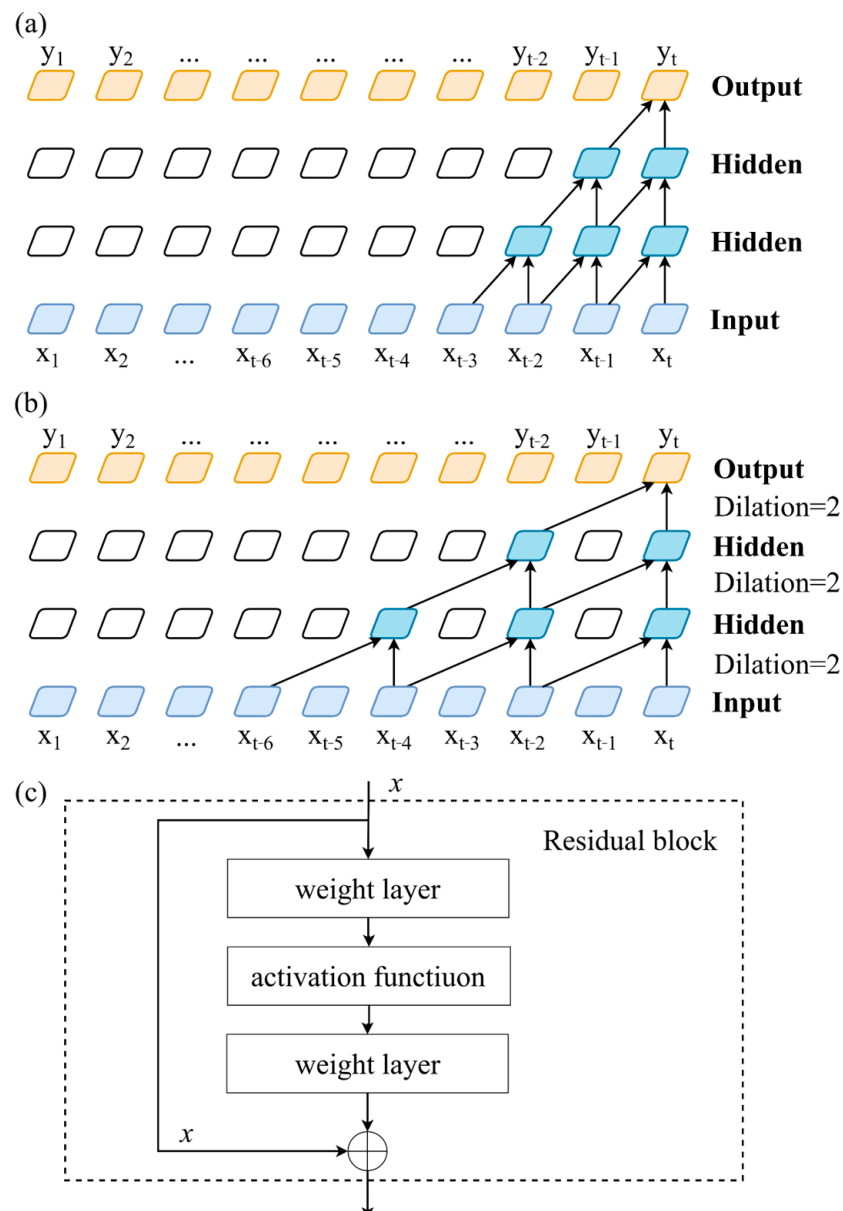


Figure 4. Architectural elements in a TCN: (a) causal convolution; (b) dilation convolution; (c) residual block.

2.3. Feature Selection Used in the TCN Method

Feature selection is critical to the performance of ML methods. Traditional methods usually utilize the current, voltage and temperature as the input data [26]. However, the estimation results fluctuate wildly and need to be further processed by other algorithms. The reason is that there is a poor correlation between the input data and SOC. In this section, the correlation between three parameters and SOC was evaluated based on the ICR18650 battery that operates at the FUDS driving cycle under 25 °C. In addition, to improve the estimation performance, a new parameter called observed SOC was introduced based on the Coulomb counting method. First, the initial state function was simplified to reduce the calculation amount [26]. Then, a degradation factor f was introduced to reduce the errors caused by temperature. Since the DST data will be used to train the ML method in this paper, they could also be utilized to calculate the degradation factor f . Finally, the observed SOC was defined as:

$$\hat{SOC}_k = \hat{SOC}_{k-1} - \frac{I_{k-1} * \Delta t}{Q_n} * f, \quad (8)$$

where I_{k-1} denotes the current at the $k-1$ time step, Δt is the change of time, and Q_n represents the nominal capacity of the battery.

The results are shown in Figure 5. The R^2 was defined through Equation (9). Among the four parameters, the observed SOC had the best correlation with the SOC. The results also prove that the temperature and voltage are highly correlated to the SOC value.

$$R^2 = 1 - \frac{\sum_{i=1}^n (y_i - \bar{x}_i)^2}{\sum_{i=1}^n (y_i - \bar{y})^2} \quad (9)$$

where y_i represents the SOC, x_i represents the input parameter, and \bar{x}_i is the average value of x_i .

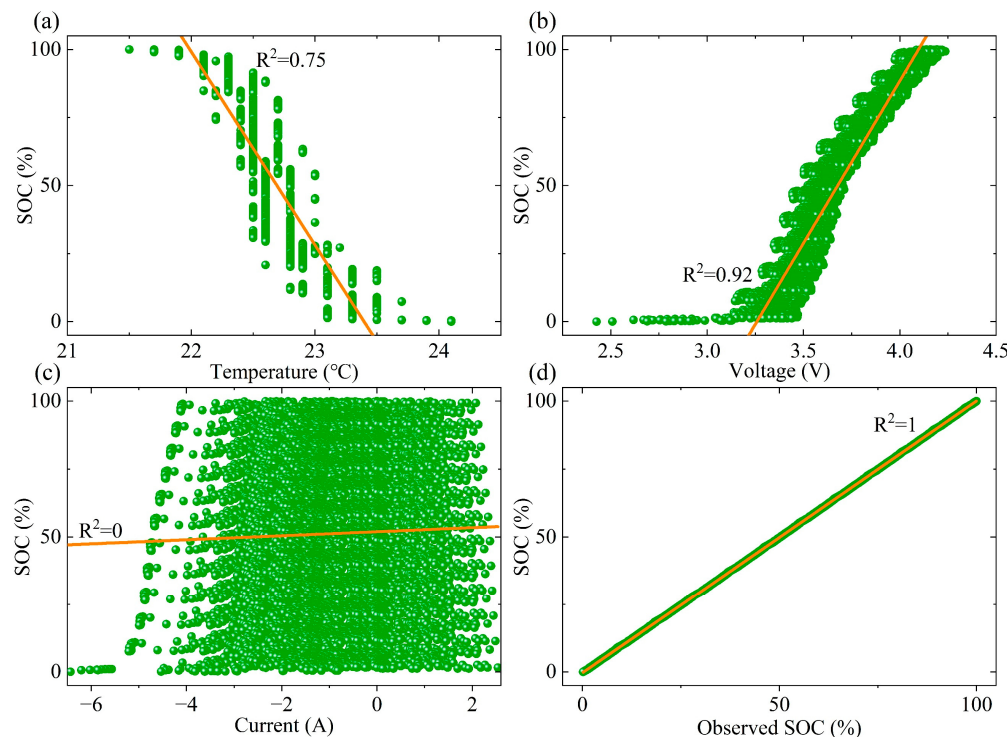


Figure 5. Correlations between four input parameters and SOC based on the ICR18650 battery when working in FUDS under 25 °C: (a) temperature, (b) voltage, (c) current, and (d) observed SOC calculated by the optimized state function.

The eight strategies of input features were evaluated by the TCN model based on the ICR18650 battery when working in the FUDS driving cycle under 25 °C (see Figure 6).

Figure 6a presents the traditional strategy, utilized current, voltage and temperature as input features, and it shows a poor estimation performance. In addition, the other strategies that use the current as an input feature also exhibit poor estimation accuracy, as shown in Figure 6c,d,g. The reason is that the current has a poor correlation to the SOC and affected the convergence of the model. In Figure 6f,h, the strategies with a single feature perform the best performance. Finally, the observed SOC was selected as the input feature according to the results in Figure 6.

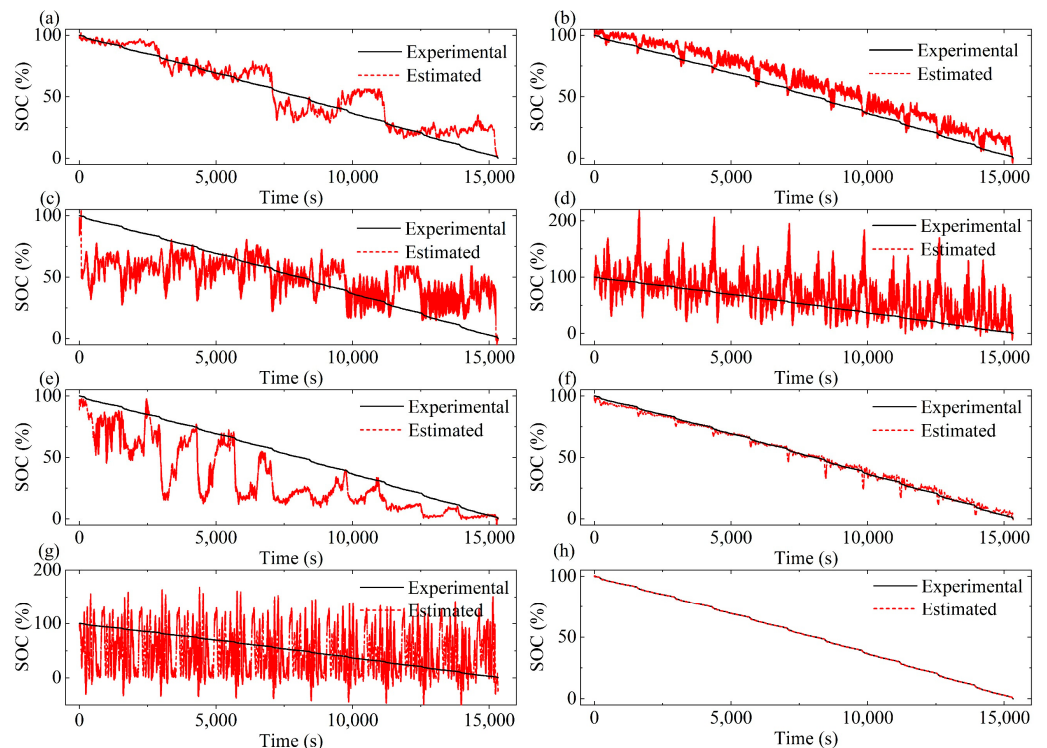


Figure 6. The SOC estimation results of the TCN model with different input parameters based on the ICR18650 battery (works at the FUDS condition under 25 °C): (a) current, voltage, and temperature; (b) voltage and temperature; (c) current and temperature; (d) current and voltage; (e) temperature; (f) voltage; (g) current; (h) observed SOC calculated by the optimized state function.

2.4. Network Structure Optimization Using the Taguchi Method

In this section, we first propose three TCNs with different architectures (see Figure 7). To find out the best architecture, the three TCNs with the relevant optimal hyperparameters were compared to each other. The DST data of ICR18650 under 25 °C were utilized to train each TCN, and the estimation performances for FUDS, UDDS and US06 data were used as the evaluation basis. Traditional methods usually employ the trial-and-error method to obtain the optimal topology; however, this approach is time-consuming and inefficient. In this paper, three design factors were settled, each of them with five levels (see Tables S4 and S5). This means that 375 groups of tests would need to be performed for all TCNs with the trial-and-error method. In contrast, the Taguchi method has proved to have a lower cost and higher efficiency for parameter optimization [53,54]; therefore, it was introduced and the number of total tests declined to 75 groups. The orthogonal array L₂₅(5³) and experimental results for three TCNs can be seen in Tables S6–S8. The best estimation results of the TCNs are concluded in Table 2. The TCN-v1 model had the minimum MAE, and the TCN-v2 model had the minimum RMSE. Since the RMSE is more sensitive to outliers, it is considered more important than the MAE. Therefore, the adopted TCN-v2 model featured 128 filters, the kernel size of 10, and the list of the dilation of {2, 2, 2, 2, 2} according to the results in Tables S6–S8.

Table 2. The SOC estimation performance for ICR18650 under 25 °C based on the three kinds of TCN (TCN-v1, TCN-v2, TCN-v3) with the relevant optimal hyperparameters.

| Neural Networks | FUDS | | UDDS | | US06 | |
|-----------------|---------|----------|---------|----------|---------|----------|
| | MAE (%) | RMSE (%) | MAE (%) | RMSE (%) | MAE (%) | RMSE (%) |
| TCN-v1 | 0.059 | 0.102 | 0.089 | 0.122 | 0.116 | 0.159 |
| TCN-v2 | 0.062 | 0.091 | 0.099 | 0.119 | 0.128 | 0.157 |
| TCN-v3 | 0.062 | 0.102 | 0.099 | 0.128 | 0.129 | 0.167 |

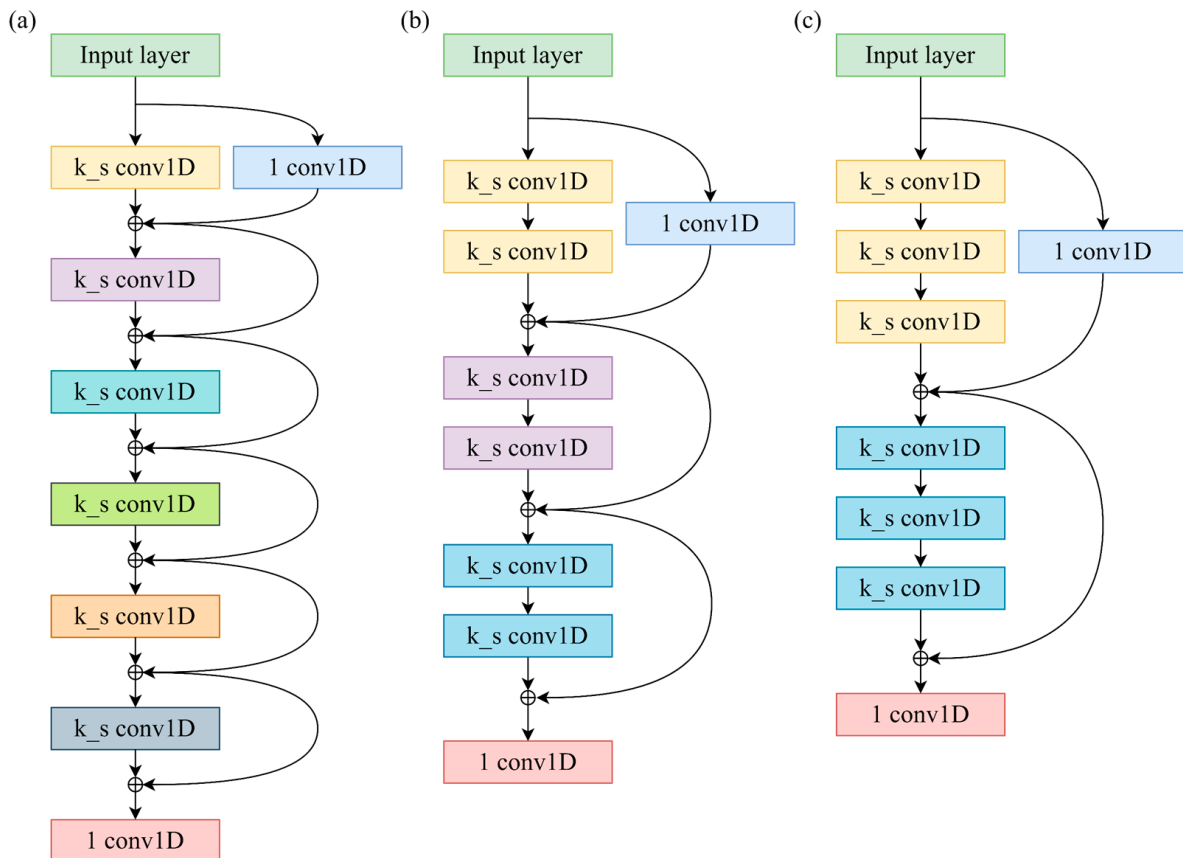


Figure 7. Architectures of TCN for SOC estimation: (a) TCN-v1; (b) TCN-v2; (c) TCN-v3.

2.5. Adaptive SOC Estimation Method

In this section, the adaptive TCN-v2 (ATCN-v2) model is proposed to estimate the battery SOC. As shown in Figure 8, the ATCN-v2 model can be divided into two parts: offline training and online estimation. Firstly, the DST data are utilized to train the optimized state function to obtain the degradation factor f . Secondly, the experimental SOC and the observed SOC calculated by the optimized state function are utilized to train the TCN model. Thirdly, the structure of the TCN is optimized based on the Taguchi method, and the TCN-v2 model is established. For the part of the online estimation, the FUDS, UDDS, and US06 data are utilized to test the model. Since the TCN-v2 has the architectural element of causal convolution, the estimation results of the first 108 s will not be accurate due to the padding operation (see Figure S1). In contrast, the optimized state function has a better performance at the initial stage of real driving cycles. Therefore, the observed SOC calculated by the optimized state function is utilized to correct the estimation results of the initial 108 s based on the TCN-v2 model. Finally, the estimated SOC is output by the ATCN-v2 model. In this study, the proposed model is developed based on the PyCharm software and TensorFlow package. The detailed training information is given in Table S9.

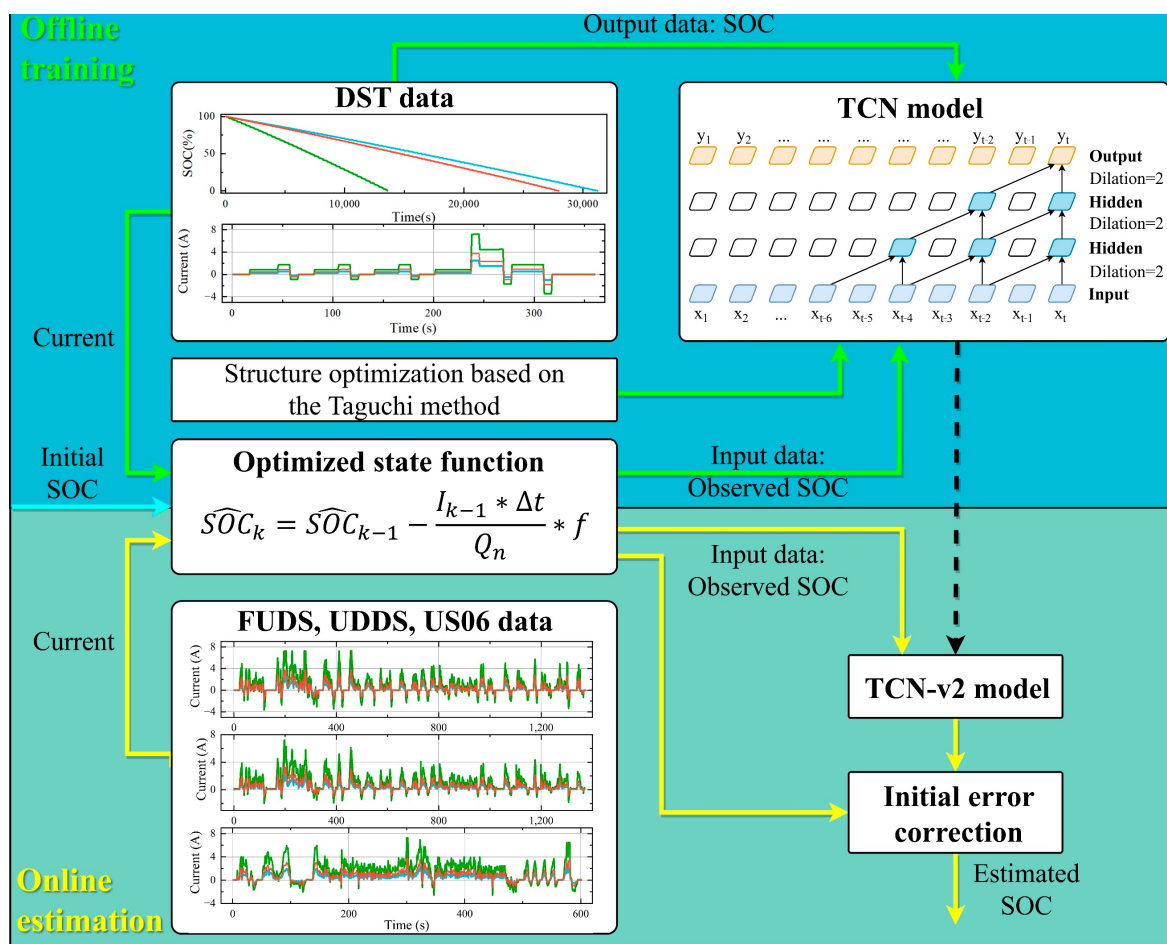


Figure 8. Graphical description of the proposed ATCN-v2 model.

3. Results and Discussion

3.1. SOC Estimation Results Based on the ATCN-v2 Model

In order to verify the performance of the ATCN-v2 model, 45 samples were utilized under different conditions, including three temperatures, three real driving cycles, and five types of batteries. The SOC estimation results of the ATCN-v2 model are shown in Figures S2–S6. They have almost no error as compared with the experimental values, which demonstrates an excellent estimation performance of the proposed method for all samples. As depicted in Figure 9, the estimation errors for all samples exhibit periodical changes. They are within $\pm 0.2\%$ for the temperature of -20°C , $\pm 0.6\%$ for the temperature of 25°C , and $\pm 0.3\%$ for the temperature of 60°C . The results further indicate that the proposed method has a good estimation performance under extreme temperatures (-20 and 60°C). Finally, the MAEs and RMSEs of the ATCN-v2 model for different types of batteries under different real driving cycles and temperatures were calculated (see Table 3). The MAEs were distributed from 0.021% to 0.185%, and the RMSEs were distributed from 0.026% to 0.277%, indicating that the proposed method has good generalizability.

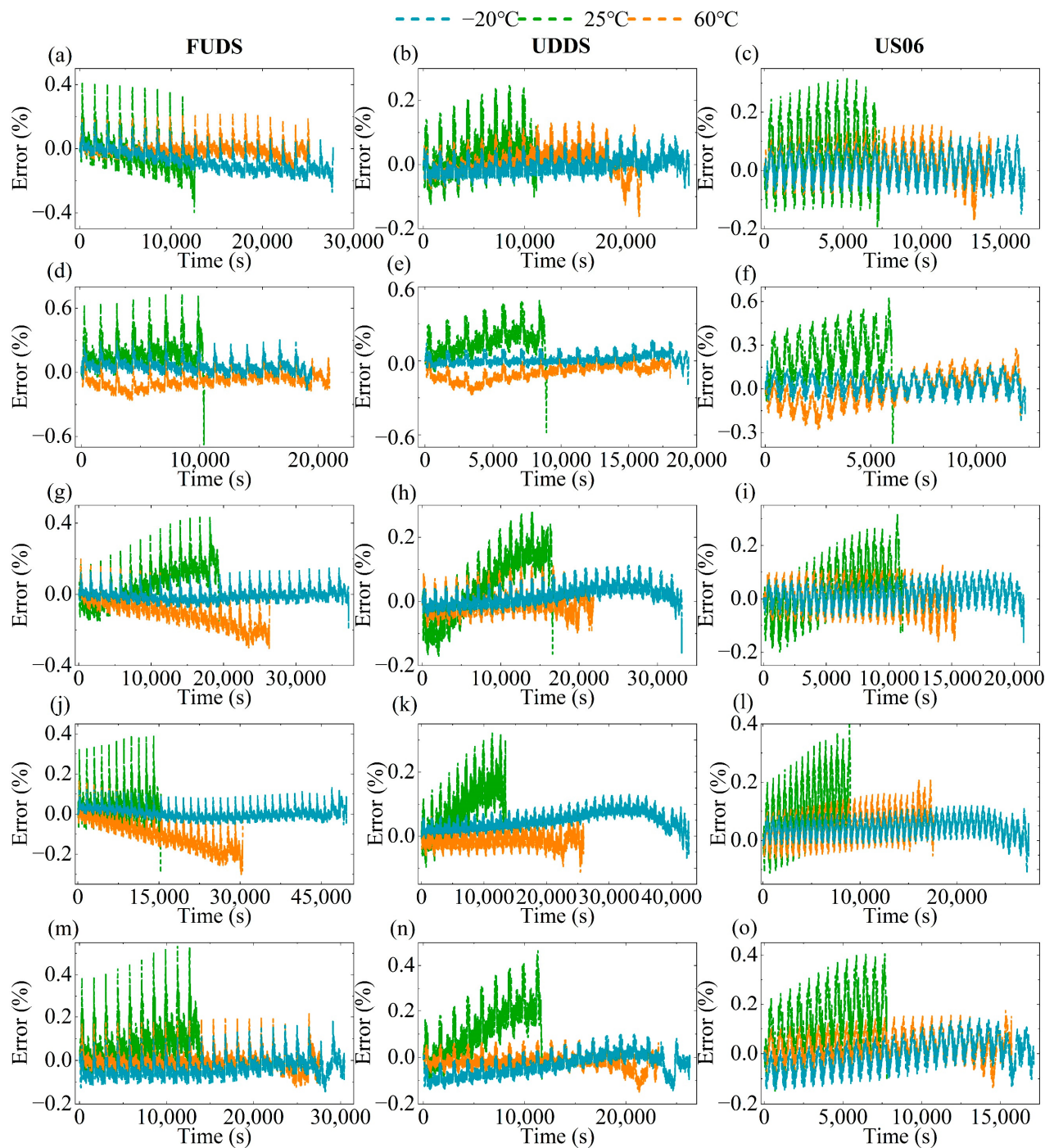


Figure 9. The estimation errors of ATCN-v2 model for different types of batteries under different conditions and temperatures: (a–c) LR1865SZ; (d–f) LR1865EH; (g–i) LR1865SK; (j–l) ICR18650; (m–o) LR2170SA.

Table 3. SOC estimation performance of the ATCN-v2 model for different types of batteries under different real driving cycles and temperatures.

| Temperature | Cases | FUDS | | UDDS | | US06 | |
|-------------|----------|---------|----------|---------|----------|---------|----------|
| | | MAE (%) | RMSE (%) | MAE (%) | RMSE (%) | MAE (%) | RMSE (%) |
| −20 °C | LR1865EH | 0.060 | 0.080 | 0.028 | 0.038 | 0.055 | 0.066 |
| | LR1865SK | 0.027 | 0.034 | 0.026 | 0.033 | 0.034 | 0.041 |
| | LR1865SZ | 0.083 | 0.097 | 0.021 | 0.026 | 0.041 | 0.048 |
| | LR2170SA | 0.049 | 0.056 | 0.047 | 0.058 | 0.049 | 0.060 |
| | ICR18650 | 0.022 | 0.029 | 0.050 | 0.056 | 0.047 | 0.055 |
| 25 °C | LR1865EH | 0.185 | 0.226 | 0.156 | 0.182 | 0.237 | 0.277 |
| | LR1865SK | 0.099 | 0.123 | 0.094 | 0.109 | 0.086 | 0.107 |
| | LR1865SZ | 0.088 | 0.113 | 0.048 | 0.064 | 0.107 | 0.132 |
| | LR2170SA | 0.094 | 0.128 | 0.127 | 0.154 | 0.145 | 0.177 |
| | ICR18650 | 0.061 | 0.090 | 0.099 | 0.118 | 0.127 | 0.156 |
| 60 °C | LR1865EH | 0.092 | 0.105 | 0.097 | 0.114 | 0.083 | 0.103 |
| | LR1865SK | 0.114 | 0.132 | 0.028 | 0.034 | 0.049 | 0.058 |
| | LR1865SZ | 0.036 | 0.051 | 0.031 | 0.040 | 0.052 | 0.064 |
| | LR2170SA | 0.034 | 0.047 | 0.029 | 0.037 | 0.051 | 0.063 |
| | ICR18650 | 0.106 | 0.123 | 0.024 | 0.029 | 0.059 | 0.073 |

3.2. Performance Evaluation

In this section, the widely used algorithms, including the LSTM, gated recurrent unit (GRU) neural network, CNN, and CNN-LSTM, were selected for comparison with the proposed ATCN-v2 model. To make the results credible, all algorithms in this paper were settled with the same random seed to avoid randomness. In addition, the algorithms used for comparison were developed with the same structure and hyperparameters as the proposed ATCN-v2 model. The criteria of algorithm evaluation involved the generalizability to temperature, conditions, battery type, and estimation accuracy. First, the MAEs and RMSEs of the LSTM, GRU, CNN, and CNN-LSTM for all 45 samples were calculated and summarized in Tables S9–S12. It can be seen that, for the LSTM, the MAEs were distributed from 0.077% to 9.020%, and the RMSEs were distributed from 0.101% to 10.483%. For the GRU, the MAEs were distributed from 0.087% to 9.196%, and the RMSEs were distributed from 0.104% to 10.599%. For the CNN, the MAEs were distributed from 0.037% to 0.391%, and the RMSEs were distributed from 0.211% to 0.829%. For the CNN-LSTM, the MAEs were distributed from 0.062% to 9.006%, and the RMSEs were distributed from 0.068% to 10.475%. When compared with these methods, the proposed method has the best accuracy. Besides, the average MAEs and average RMSEs of all algorithms were also depicted in Figure 10 for visual comparison. The LSTM, GRU and CNN-LSTM showed poor adaptation to battery type and temperature. For example, they produced abnormally large errors for the battery LR1865EH working under an extreme temperature of −20 °C, for the battery LR2170SA working under 25 °C, and for the battery LR1865SZ working under an extreme temperature of 60 °C. Among them, the proposed method obtained the highest accuracy and the best adaptation to battery type and temperature. Finally, the average MAEs and average RMSEs of five algorithms for the total 45 samples were calculated as shown in Table 4. The performances of LSTM, GRU and CNN-LSTM are very similar. When compared with these methods, the CNN exhibited better performance. Among them, the optimal algorithm was still the ATCN-v2, and its average MAE showed a decline of at least 49.66%, and the average RMSE exhibited a decline of at least 79.95%.

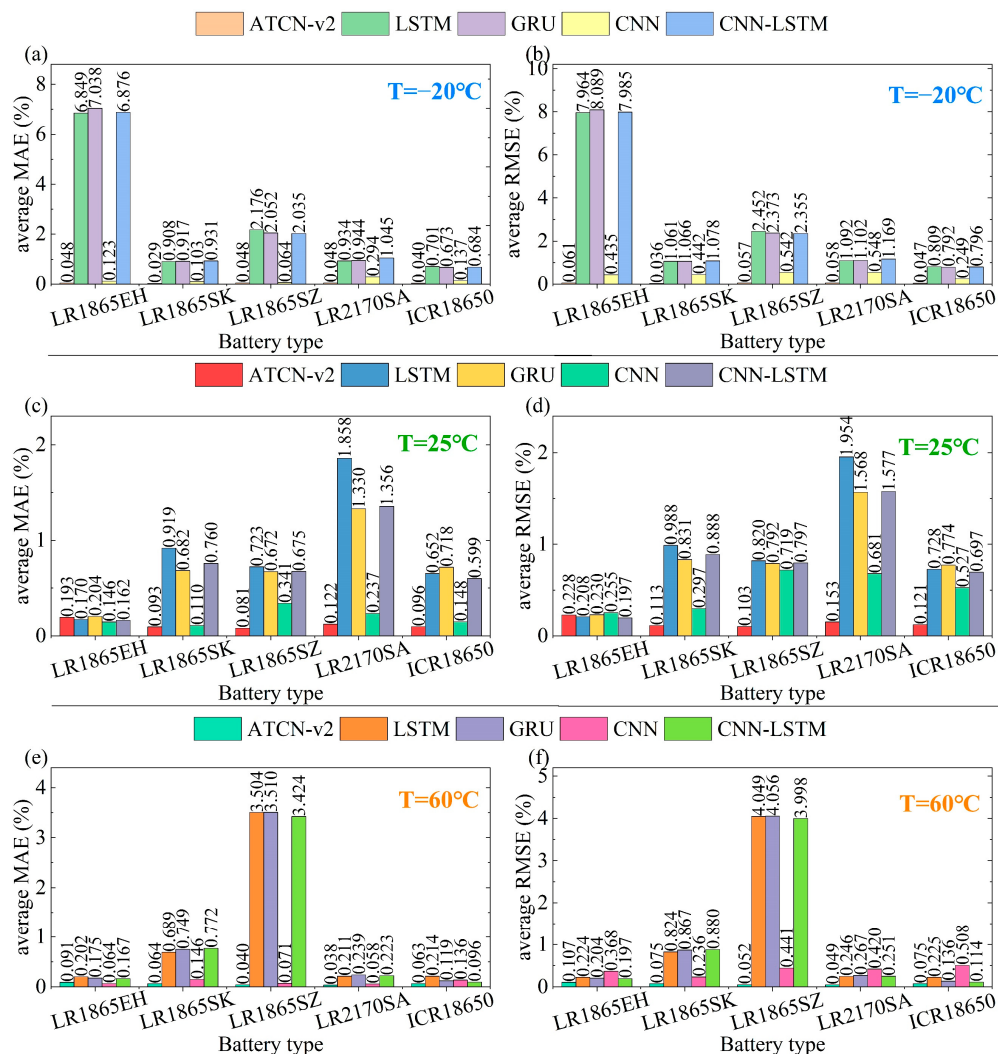


Figure 10. SOC estimation errors of the different algorithms for five types of batteries (LR1865EH, LR1865SK, LR1865SZ, LR2170SA, and ICR18650): (a,b) average MAE and average RMSE under -20°C ; (c,d) average MAE and average RMSE under 25°C ; (e,f) average MAE and average RMSE under 60°C .

Table 4. SOC estimation performance of the different algorithms.

| Algorithm | Average MAE (%) | Average RMSE (%) |
|-----------|-----------------|------------------|
| ATCN-v2 | 0.073 | 0.089 |
| LSTM | 1.381 | 1.576 |
| GRU | 1.335 | 1.543 |
| CNN | 0.145 | 0.444 |
| CNN-LSTM | 1.320 | 1.532 |

In order to further quantify the generalizability of algorithms, the standard deviations (SDs) of estimation errors (i.e., MAEs and RMSEs) were calculated, that is, to evaluate if the algorithms performed stably when only one parameter (i.e., temperature, driving cycle, or battery type) was changed. The standard deviation was defined as:

$$\sigma = \sqrt{\frac{1}{n} \sum_{i=1}^n (X_i - \bar{X})^2} \quad (10)$$

where X_i represents the SOC estimation error, and \bar{X} represents the average error.

The final results are summarized in Table 5. The adaptation was evaluated for three kinds of parameters, namely, temperature, driving cycle, and battery type. Among them, five algorithms proved to be more adaptable to the different driving cycles, and their performances for different battery types or different temperatures were highly unstable. The traditional methods including LSTM, GRU and CNN-LSTM provided the worst generalizability compared with the proposed method and CNN. The SDs of all the MAEs and RMSEs were calculated as the comprehensive index to evaluate the generalizability of algorithms. The SD of MAEs can be utilized to measure the change of entire errors, and the SD of RMSEs can be utilized to measure the change of the discrete degree of errors. Hence, the smaller the SD of MAEs and SD of RMSEs, the better the generalizability of the algorithm. The SDs of MAEs and RMSEs were 0.046 and 0.055 for the ATCN-v2, 1.862 and 2.160 for LSTM, 1.897 and 2.185 for GRU, 0.085 and 0.152 for CNN, and 1.857 and 2.159 for CNN-LSTM, respectively. Thus, the ATCN-v2 model was indicated to have the best generalizability as compared to other methods.

Table 5. SOC estimation performance of the ATCN-v2 model for different types of batteries under different real driving cycles and temperatures.

| Parameter | Algorithm | The SD of MAE (%) | The SD of RMSE (%) |
|---------------|-----------|-------------------|--------------------|
| Temperature | ATCN-v2 | 0.037 | 0.044 |
| | LSTM | 1.245 | 1.430 |
| | GRU | 1.237 | 1.427 |
| | CNN | 0.064 | 0.102 |
| | CNN-LSTM | 1.215 | 1.413 |
| Driving cycle | ATCN-v2 | 0.018 | 0.019 |
| | LSTM | 0.548 | 0.630 |
| | GRU | 0.543 | 0.627 |
| | CNN | 0.022 | 0.048 |
| | CNN-LSTM | 0.535 | 0.622 |
| Battery type | ATCN-v2 | 0.027 | 0.031 |
| | LSTM | 1.433 | 1.640 |
| | GRU | 1.407 | 1.620 |
| | CNN | 0.068 | 0.131 |

The effects of temperature on the performance of algorithms were also analyzed. In Table 6, the stability of algorithms under different temperatures without considering the battery type and driving cycle was evaluated by the standard deviation of estimation errors (i.e., MAE and RMSE). The traditional methods, including LSTM, GRU and CNN-LSTM, obtained the largest standard deviation of MAE and RMSE for the battery working at an extremely low temperature (-20°C), and also had a larger standard deviation of MAE and RMSE for the battery working at an extremely high temperature (60°C), which declined by more than 50% compared to that when working at 25°C . In other words, these methods result in large errors when used for estimating the SOC of batteries operating at extreme temperatures (-20 and 60°C). Among the five algorithms, the ATCN-v2 model had the minimum standard deviation of MAE and RMSE at three temperatures ($-20, 25, 60^{\circ}\text{C}$). The results also indicate that the proposed method is suitable for SOC estimation at extreme temperatures (-20 and 60°C). We also noticed that the ATCN-v2 model had a faster convergence velocity compared to the LSTM, GRU and CNN-LSTM. In the same computing environment, the ATCN-v2 method needed about 300 epochs to achieve convergence; meanwhile, the LSTM, GRU and CNN-LSTM required about 500 epochs.

Table 6. The stability of algorithms under different temperatures.

| Algorithms | −20 °C | | 25 °C | | 60 °C | |
|------------|-------------------|--------------------|-------------------|--------------------|-------------------|--------------------|
| | The SD of MAE (%) | The SD of RMSE (%) | The SD of MAE (%) | The SD of RMSE (%) | The SD of MAE (%) | The SD of RMSE (%) |
| ATCN-v2 | 0.092 | 0.105 | 0.097 | 0.114 | 0.083 | 0.103 |
| LSTM | 0.114 | 0.132 | 0.028 | 0.034 | 0.049 | 0.058 |
| GRU | 0.036 | 0.051 | 0.031 | 0.040 | 0.052 | 0.064 |
| CNN | 0.034 | 0.047 | 0.029 | 0.037 | 0.051 | 0.063 |
| CNN-LSTM | 0.106 | 0.123 | 0.024 | 0.029 | 0.059 | 0.073 |

4. Conclusions

This work proposed a new algorithm based on the TCN and Coulomb counting method for estimating the SOC of five types of LIBs. First, different parameters, including current, voltage, temperature, and observed SOC, were evaluated for suitability as the input data of the model. Eight strategies for input data were designed, and the strategies with a single and highly SOC-related parameter showed the best performance. Therefore, the observed SOC calculated by optimized state function was selected as the input data. Then, three TCNs with different structures were compared to find the best scheme, whose structure was optimized by the Taguchi method. Considering that there are initial errors caused by the padding operation, the estimation results of the first 108 time steps were corrected. Finally, the ATCN-v2 model was established.

In order to better verify the accuracy and generalizability of the proposed algorithm, five types of widely used batteries composed of three kinds of cathode materials (i.e., LiFePO₄, Li(Ni_{0.5}Co_{0.2}Mn_{0.3})O₂, and LiCoO₂) were tested under four real driving cycles and three temperatures. The real driving cycles included DST, FUDS, UDDS, and US06. The test temperatures include an extremely low temperature (−20 °C), an extremely high temperature (60 °C) for the mentioned batteries above, and a constant temperature of 25 °C. Finally, 60 groups of real driving cycle tests were developed. The DST data were utilized for model training, and FUDS data, UDDS data and US06 data were utilized for model testing. The SOC estimation errors of the ATCN-v2 model were within ±0.6%, and the MAEs and RMSEs were less than 0.185% and 0.277%, respectively. Subsequently, the proposed method was compared with four popular algorithms, including LSTM, GRU, CNN and CNN-LSTM. The algorithms adopted the same structure, input data and hyperparameters. The average MAE of the ATCN-v2 model declined by at least 49.66%, and the average RMSE declined by at least 79.95% when compared to other methods. The results indicate that the proposed method has the highest estimation accuracy.

In addition, the SDs of MAEs and RMSEs were calculated to quantify the generalizability of the algorithms. Three experimental variables could be considered to test the generalization ability, which comprise battery type, real driving cycle and temperature. First, the generalization ability to an individual variable of the algorithms was evaluated. The results show that it is hard to adapt to different types of batteries and different temperatures for the LSTM, GRU and LSTM-CNN. The proposed model exhibited the best generalization ability to any of these variables with the minimum SDs of MAEs and RMSEs. The effects of different temperatures on the algorithm performance were also studied in this way. The results suggest that extremely low temperature (−20 °C) and extremely high temperature (60 °C) for the batteries in this paper have a significant impact on the performance of LSTM, GRU and CNN-LSTM, while the ATCN-v2 method is highly adaptable to these two extreme temperatures. Finally, the comprehensive generalization ability to three experimental variables was obtained by computing the SDs of all of the MAEs and RMSEs. Compared to other methods, the SDs of MAEs and RMSEs of the ATCN-v2 method dropped by at least 45.88% and 63.82%, respectively. In summary, the proposed ATCN-v2 method demonstrated excellent SOC estimation accuracy and good generalization ability, and had better performance and stability of battery operation for all battery types, and

also real driving cycles under extreme temperatures, as compared with LSTM, GRU, CNN and CNN-LSTM. In further research, we will consider applying the ATCN-v2 to a larger dataset. The proposed method can be helpful to accelerate the research and application process in battery energy storage and green transport.

Supplementary Materials: The following supporting information can be downloaded at: <https://www.mdpi.com/article/10.3390/batteries8100145/s1>.

Author Contributions: Conceptualization, J.M. (Jiazh Miao) and Z.T.; methodology, J.M. (Jiazh Miao); software, Z.T. and S.T.; validation, J.M. (Jiazh Miao) and J.Z.; investigation, Z.T. and J.M. (Jiale Mao); resources, S.T.; data curation, J.Z.; writing—original draft preparation, J.M. (Jiazh Miao); writing—review and editing, Z.T. and J.M. (Jiazh Miao); project administration, S.T.; funding acquisition, Z.T. All authors have read and agreed to the published version of the manuscript.

Funding: This research was funded by the National Natural Science Foundation of China (52075481) and Zhejiang Provincial Natural Science Foundation (LR19E050002).

Data Availability Statement: The inventory used in this study is available upon request from the corresponding author.

Conflicts of Interest: The authors declare no conflict of interest.

References

1. Hu, X.; Xu, L.; Lin, X.; Pechet, M. Battery lifetime prognostics. *Joule* **2020**, *4*, 310. [[CrossRef](#)]
2. Sulaiman, N.; Hannan, M.A.; Mohamed, A.; Majlan, E.H.; Wan Daud, W.R. A review on energy management system for fuel cell hybrid electric vehicle: Issues and challenges. *Renew. Sustain. Energy Rev.* **2015**, *52*, 802. [[CrossRef](#)]
3. Zhang, Q.; Tong, Z.; Tong, S.; Cheng, Z. Modeling and dynamic performance research on proton exchange membrane fuel cell system with hydrogen cycle and dead-ended anode. *Energy* **2021**, *218*, 119476. [[CrossRef](#)]
4. Zhang, Q.; Tong, Z.; Tong, S. Effect of cathode recirculation on high potential limitation and self-humidification of hydrogen fuel cell system. *J. Power Sources* **2020**, *468*, 228388. [[CrossRef](#)]
5. Rietmann, N.; Hügler, B.; Lieven, T. Forecasting the trajectory of electric vehicle sales and the consequences for CO₂ emissions. *J. Clean. Prod.* **2020**, *261*, 121038. [[CrossRef](#)]
6. Li, Y.; Liu, K.; Foley, A.M.; Zülke, A.; Berecibar, M.; Nanini-Maury, E.; Mierlo, J.V.; Hoster, H.E. Data-driven health estimation and lifetime prediction of lithium-ion batteries: A review. *Renew. Sust. Energ. Rev.* **2019**, *113*, 109254. [[CrossRef](#)]
7. Zhang, W.; Fan, L.; Tong, Z.; Miao, J.; Shen, Z.; Li, S.; Chen, F.; Qiu, Y.; Lu, Y. Stable Li-metal deposition via a 3D nanodiamond matrix with ultrahigh young's modulus. *Small Methods* **2019**, *3*, 1900325. [[CrossRef](#)]
8. Tong, Z.; Miao, J.; Li, Y.; Tong, S.; Zhang, Q.; Tan, G. Development of electric construction machinery in China: A review of key technologies and future directions. *J. Zhejiang Univ.-SCI. A* **2021**, *22*, 245–264. [[CrossRef](#)]
9. Shen, J.; Ma, W.; Xiong, J.; Shu, X.; Zhang, Y.; Chen, Z.; Liu, Y. Alternative combined co-estimation of state of charge and capacity for lithium-ion batteries in wide temperature scope. *Energy* **2022**, *244*, 123236. [[CrossRef](#)]
10. Rahman, A.; Lin, X. Li-ion battery individual electrode state of charge and degradation monitoring using battery casing through auto curve matching for standard CCCV charging profile. *Appl. Energy* **2022**, *321*, 119367. [[CrossRef](#)]
11. Tian, J.; Xiong, R.; Shen, W.; Lu, J. State-of-charge estimation of LiFePO₄ batteries in electric vehicles: A deep-learning enabled approach. *Appl. Energy* **2021**, *291*, 116812. [[CrossRef](#)]
12. Kröger, T.; Harte, P.; Klein, S.; Beuse, T.; Börner, M.; Winter, M.; Nowak, S.; Wiemers-Meyer, S. Direct investigation of the interparticle-based state-of-charge distribution of polycrystalline NMC532 in lithium ion batteries by classification-single-particle-ICP-OES. *J. Power Sources* **2022**, *527*, 231204. [[CrossRef](#)]
13. Zhang, Q.; Tong, Z.; Tong, S. Research on the influence of electrolytes on the low-temperature start-up performance of zinc-air battery for forklifts. *Int. J. Energy Res.* **2022**, *46*, 10169–10181. [[CrossRef](#)]
14. Chen, Z.; Zhou, J.; Zhou, F.; Xu, S. State-of-charge estimation of lithium-ion batteries based on improved H infinity filter algorithm and its novel equalization method. *J. Clean. Prod.* **2021**, *290*, 125180. [[CrossRef](#)]
15. Tian, J.; Xiong, R.; Shen, W.; Sun, F. Electrode ageing estimation and open circuit voltage reconstruction for lithium ion batteries. *Energy Storage Mater.* **2021**, *37*, 283–295. [[CrossRef](#)]
16. Wang, Y.; Zhang, C.; Chen, Z. A method for state-of-charge estimation of Li-ion batteries based on multi-model switching strategy. *Appl. Energy* **2015**, *137*, 427–434. [[CrossRef](#)]
17. Tong, Z.; Miao, J.; Mao, J.; Wang, Z.; Lu, Y. Prediction of Li-ion battery capacity degradation considering polarization recovery with a hybrid ensemble learning mode. *Energy Storage Mater.* **2022**, *50*, 533–542. [[CrossRef](#)]
18. Hannan, M.A.; Lipu, M.S.H.; Hussain, A.; Mohamed, A. A review of lithium-ion battery state of charge estimation and management system in electric vehicle applications: Challenges and recommendations. *Renew. Sust. Energ. Rev.* **2017**, *78*, 834. [[CrossRef](#)]

19. Wang, X.; Sun, Q.; Kou, X.; Ma, W.; Zhang, H.; Liu, R. Noise immune state of charge estimation of li-ion battery via the extreme learning machine with mixture generalized maximum correntropy criterion. *Energy* **2022**, *239*, 122406. [[CrossRef](#)]
20. Tong, Z.; Yang, Q.; Tong, S.; Chen, X. Two-stage thermal-hydraulic optimization for Pillow Plate Heat Exchanger with recirculation zone parameterization. *Appl. Therm. Eng.* **2022**, *215*, 119033. [[CrossRef](#)]
21. Wang, S.; Fernandez, C.; Yu, C.; Fan, Y.; Cao, W.; Stroe, D. A novel charged state prediction method of the lithium ion battery packs based on the composite equivalent modeling and improved splice Kalman filtering algorithm. *J. Power Sources* **2020**, *471*, 228450. [[CrossRef](#)]
22. Snihir, I.; Rey, W.; Verbitskiy, E.; Belfadhel-Ayeb, A.; Notten, P.H.L. Battery open-circuit voltage estimation by a method of statistical analysis. *J. Power Sources* **2006**, *159*, 1484–1487. [[CrossRef](#)]
23. Ng, K.S.; Moo, C.S.; Chen, Y.P.; Hsieh, Y.C. Enhanced coulomb counting method for estimating state-of-charge and state-of-health of lithium-ion batteries. *Appl. Energy* **2009**, *86*, 1506–1511. [[CrossRef](#)]
24. Li, M. Li-ion dynamics and state of charge estimation. *Renew. Energy* **2017**, *100*, 44–52. [[CrossRef](#)]
25. Xiong, R.; Li, L.; Yu, Q.; Jin, Q.; Yang, R. A set membership theory based parameter and state of charge co-estimation method for all-climate batteries. *J. Clean. Prod.* **2020**, *249*, 119380. [[CrossRef](#)]
26. Wang, S.; Fernandez, C.; Zou, C.; Yu, C.; Li, X.; Pei, S.; Xie, W. Open circuit voltage and state of charge relationship functional optimization for the working state monitoring of the aerial lithium-ion battery pack. *J. Clean. Prod.* **2018**, *198*, 1090–1104. [[CrossRef](#)]
27. Tian, Y.; Lai, R.; Li, X.; Xiang, X.; Tian, J. A combined method for state-of-charge estimation for lithium-ion batteries using a long short-term memory network and an adaptive cubature Kalman filter. *Appl. Energy* **2020**, *265*, 114789. [[CrossRef](#)]
28. Zheng, L.; Zhang, L.; Zhu, J.; Wang, G.; Jiang, J. Co-estimation of state-of-charge, capacity and resistance for lithium-ion batteries based on a high-fidelity electrochemical model. *Appl. Energy* **2016**, *180*, 424–434. [[CrossRef](#)]
29. Zheng, Y.; Ouyang, M.; Han, X.; Lu, L.; Li, J. Investigating the error sources of the online state of charge estimation methods for lithium-ion batteries in electric vehicles. *J. Power Sources* **2018**, *377*, 161–188. [[CrossRef](#)]
30. Chen, Z.; Sun, H.; Dong, G.; Wei, J.; Wu, J. Particle filter-based state-of-charge estimation and remaining-dischargeable-time prediction method for lithium-ion batteries. *J. Power Sources* **2019**, *414*, 158–166. [[CrossRef](#)]
31. Peng, J.; Luo, J.; He, H.; Lu, B. An improved state of charge estimation method based on cubature Kalman filter for lithium-ion batteries. *Appl. Energy* **2019**, *253*, 113520. [[CrossRef](#)]
32. Ren, H.; Zhang, H.; Gao, Z.; Zhao, Y. A robust approach to state of charge assessment based on moving horizon optimal estimation considering battery system uncertainty and aging condition. *J. Clean. Prod.* **2020**, *270*, 122508. [[CrossRef](#)]
33. Xiong, B.; Zhao, J.; Wei, Z.; Skyllas-Kazacos, M. Extended Kalman filter method for state of charge estimation of vanadium redox flow battery using thermal-dependent electrical model. *J. Power Sources* **2014**, *262*, 50–61. [[CrossRef](#)]
34. Wang, L.; Ma, J.; Zhao, X.; Li, X.; Zhang, K.; Jiao, Z. Adaptive robust unscented Kalman filter-based state-of-charge estimation for lithium-ion batteries with multi-parameter updating. *Electrochim. Acta* **2022**, *426*, 140760. [[CrossRef](#)]
35. Yang, X.; Wang, S.; Xu, W.; Qiao, J.; Yu, C.; Takyi-Aninakwa, P.; Jin, S. A novel fuzzy adaptive cubature Kalman filtering method for the state of charge and state of energy co-estimation of lithium-ion batteries. *Electrochim. Acta* **2022**, *415*, 140241. [[CrossRef](#)]
36. Wang, Y.; Zhang, C.; Chen, Z. A method for state-of-charge estimation of LiFePO₄ batteries at dynamic currents and temperatures using particle filter. *J. Power Sources* **2015**, *279*, 306–311. [[CrossRef](#)]
37. Liu, Y.; Guo, B.; Zou, X.; Li, Y.; Shi, S. Machine learning assisted materials design and discovery for rechargeable batteries. *Energy Storage Mater.* **2020**, *31*, 434–450. [[CrossRef](#)]
38. Zhao, J.; Xu, W.; Kuang, Z.; Long, R.; Liu, Z.; Liu, W. Segmental material design in thermoelectric devices to boost heat-to-electricity performance. *Energ. Conv. Manag.* **2021**, *247*, 114754. [[CrossRef](#)]
39. Tian, J.; Xiong, R.; Lu, J.; Chen, C.; Shen, W. Battery state-of-charge estimation amid dynamic usage with physics-informed deep learning. *Energy Storage Mater.* **2022**, *50*, 718–729. [[CrossRef](#)]
40. Xu, J.; Zhen, A.; Cai, Z.; Wang, P.; Gao, K.; Jiang, D. State of health diagnosis and remaining useful life prediction of lithium-ion batteries based on multi-feature data and mechanism fusion. *IEEE Access* **2021**, *9*, 85431–85441. [[CrossRef](#)]
41. Tong, Z.; Miao, J.; Tong, S.; Lu, Y. Early prediction of remaining useful life for Lithium-ion batteries based on a hybrid machine learning method. *J. Clean. Prod.* **2021**, *317*, 128265. [[CrossRef](#)]
42. Hu, J.N.; Hu, J.J.; Lin, H.B.; Li, X.P.; Jiang, C.L.; Qiu, X.H.; Li, W.S. State-of-charge estimation for battery management system using optimized support vector machine for regression. *J. Power Sources* **2014**, *269*, 682–693. [[CrossRef](#)]
43. Chemali, E.; Kollmeyer, P.J.; Preindl, M.; Ahmed, R.; Emadi, A. Long short-term memory networks for accurate state-of-charge estimation of Li-ion batteries. *IEEE Trans. Ind. Electron.* **2018**, *65*, 6730–6739. [[CrossRef](#)]
44. Zhu, J.; Chen, N.; Peng, W. Estimation of bearing remaining useful life based on multiscale convolutional neural network. *IEEE Trans. Ind. Electron.* **2018**, *66*, 3208–3216. [[CrossRef](#)]
45. Lu, L.; Jin, P.; Pang, G.; Zhang, Z.; Karniadakis, G.E. Learning nonlinear operators via DeepONet based on the universal approximation theorem of operators. *Nat. Mach. Intell.* **2021**, *3*, 218–229. [[CrossRef](#)]
46. Cao, Y.; Ding, Y.; Jia, M.; Tian, R. A novel temporal convolutional network with residual self-attention mechanism for remaining useful life prediction of rolling bearings. *Reliab. Eng. Syst. Saf.* **2021**, *215*, 107813. [[CrossRef](#)]
47. Liu, Y.; Li, J.; Zhang, G.; Hua, B.; Xiong, N. State of charge estimation of lithium-ion batteries based on temporal convolutional network and transfer learning. *IEEE Access* **2021**, *9*, 34177–34187. [[CrossRef](#)]

48. Jagtap, A.D.; Kawaguchi, K.; Karniadakis, G.E. Adaptive activation functions accelerate convergence in deep and physics-informed neural networks. *J. Comput. Phys.* **2020**, *404*, 109136. [[CrossRef](#)]
49. Jagtap, A.D.; Kawaguchi, K.; Karniadakis, G.E. Locally adaptive activation functions with slope recovery for deep and physics-informed neural networks. *Proc. R. Soc. A-Math. Phys. Eng. Sci.* **2020**, *476*, 20200334. [[CrossRef](#)]
50. Jagtap, A.D.; Shin, Y.; Kawaguchi, K.; Karniadakis, G.E. Deep Kronecker neural networks: A general framework for neural networks with adaptive activation functions. *Neurocomputing* **2022**, *468*, 165–180. [[CrossRef](#)]
51. Lipu, M.S.H.; Hannan, M.A.; Hussain, A.; Ayob, A.; Saad, M.H.M.; Karim, T.F.; How, D.N.T. Data-driven state of charge estimation of lithium-ion batteries: Algorithms, implementation factors, limitations and future trends. *J. Clean. Prod.* **2020**, *277*, 124110. [[CrossRef](#)]
52. United States Advanced Battery Consortium. *Electric Vehicle Battery Test Procedures Manual*; USABC: Southfield, MI, USA, 1996.
53. Peace, G.S. *Taguchi Methods: A Hands-On Approach*; Addison Wesley Publishing Company: Boston, MA, USA, 1993.
54. Zhao, W.; Gao, Y.; Ji, T.; Wan, X.; Ye, F.; Bai, G. Deep temporal convolutional networks for short-term traffic flow forecasting. *IEEE Access* **2019**, *7*, 114496–114507. [[CrossRef](#)]